aerospace

MDPI

Article

The Confirmation of Thermal Boundary Parameters in an Oxygen Kerosene Fuel-Rich Rocket Engine

Xianggeng Wei [1], Zhongxu Yang [1], Shaohua Zhu [1,*], Zhixin Zhao [1], Jinying Ye [1] and Oskar J. Haidn [2]

[1] Science and Technology on Combustion, Internal Flow and Thermo-Structure Laboratory, Northwestern Polytechnical University, Xi'an 710072, China; realysnow@nwpu.edu.cn (X.W.); yzxbd@mail.nwpu.edu.cn (Z.Y.); chenxiing@mail.nwpu.edu.cn (Z.Z.); yjy@nwpu.edu.cn (J.Y.)
[2] Institute of Turbomachinery and Flight Propulsion, Technical University of Munich, 85748 Garching, Germany; oskar.haidn@tum.de
* Correspondence: zhushaohua@nwpu.edu.cn

Abstract: The thermal environment is an important factor in the design of liquid rockets. In this paper, theoretical analysis, numerical simulation and experimental testing are conducted to study the boundary thermal characteristics of a GOX/kerosene liquid rocket motor with a total flow rate of 120 g/s and an oxygen-fuel ratio of 1:1. We measured the axial temperature in different positions in the combustor using thermocouples and the heat flux using a flux meter. We found that the heat flux at 182 mm increases by 6.8% when a carbon deposit exists. For the theoretical results, after correcting the thermal conductivity by the volume fraction of carbon deposition, the theoretical heat flux (1.11 MW/m^2, using the corrected thermal conductivity) and the numerical result (0.89 MW/m^2, considering the injectors) are similar to the experimental value (0.937 MW/m^2). This study validates the accuracy of theoretical and simulation calculation in this case, and provides verification data for future numerical calculation, as well as data for setting gas temperature at the wall in the simulation of the gas phase.

Keywords: gas-oxygen kerosene; fuel-rich; heat flux; near-wall gas temperature

Citation: Wei, X.; Yang, Z.; Zhu, S.; Zhao, Z.; Ye, J.; Haidn, O.J. The Confirmation of Thermal Boundary Parameters in an Oxygen Kerosene Fuel-Rich Rocket Engine. *Aerospace* **2022**, *9*, 343. https://doi.org/10.3390/aerospace9070343

Academic Editor: Justin Hardi

Received: 6 April 2022
Accepted: 24 June 2022
Published: 26 June 2022

1. Introduction

Studying the thermal effect of gas on the engine wall plays a key role in the design of liquid rocket engines. In the design stage, accurately predicting the wall temperature of a rocket engine can help to design efficient cooling methods, especially for reusable engines, which can further predict their life cycle [1,2]. However, due to the complexity of the mechanism and although much research has already been carried out on the mechanism of heat transfer in the combustion chamber, especially the mechanism of heat transfer between gas and solid, there is no systematic model for the mechanism of gas and engine wall in each type of liquid rocket engine and the existing models can only play a predictive role.

Suslov et al. [3] studied the heat transfer characteristics near the injector region of the chamber wall, considering the interaction between the injector and the wall. Arnold et al. [4] carried out an experiment with a hydrogen film cooling ultra-small rocket combustor and obtained the axial and circumferential wall heat load. Taiping et al. [5] carried out an experiment about the film cooling near the injector with a GH2/GO2 heat-sink combustor and measured the wall heat flux and wall temperature distribution under different chamber pressures and propellant proportions. Marco Pizzarelli et al. [6] established a two-dimensional model for liquid oxygen/methane engines (outflow cooling) and estimated it by simulation. It was found that the wall heat flux, gas temperature and gas side wall temperature calculated by the Bartz formula were higher than the simulation results (about 10–20%). Lai et al. [7] studied the convective heat transfer between the combustion chamber wall, gas and the flow of coolant into the regenerative cooling passage by using fluid–solid coupling numerical simulation, in which the interface between solid

and fluid was treated as a coupling wall. Negishi et al. [8] and Song et al. [9] carried out heat transfer simulation in a LOX/GH2 sub-scale thrust chamber. The conceptual model of eddy current dissipation and the non-adiabatic flame model are used in the simulation. The results show that the complex heat load on the combustion chamber wall is caused by the near-wall injection components. Betti [10] established a model which can effectively predict the wall temperature, heat flux and coolant pressure loss of regenerative cooling in a liquid rocket engine. The two-dimensional model was calculated by using a CFD solver. By comparing it with the experiment, it was found that the maximum wall temperature was close to the experimental value. Celano et al. [11] studied the heat transfer process of gas-oxygen/methane propellant combination in a single-component coaxial shear nozzle combustor. The results of experiment and simulation were compared. It was found that the heat flux calculated by a one-dimensional model is higher than that calculated by simulation, and the results of a three-dimensional model are the closest to those obtained by experiment. D. Suslov et al. [12] carried out experimental and numerical simulation studies on heat transfer characteristics of the combustion chamber wall in liquid oxygen (LOX)/liquid methane (LCH4) rocket engines. They found that the simulation results were consistent with the actual situation in trend, the deviation of pressure was less than 1%, whereas the deviation of heat flux is higher than the experimental situation. Peter C. Ma et al. [13] validated a flame-based combustion model by using direct numerical simulation (DNS) to predict gas temperature, gas composition and heat transfer of gas to the engine wall. Maestro D et al. [14,15] found that predicting wall heat flux in rocket chamber structures requires the correct flow and flame models, including the chemical flame structure, gas composition and wall temperature gradient. The large eddy simulation was used to calculate the combustion, and the results were in good agreement with the experimental measurements of wall heat flux and chamber pressure. The relationship between heat released by flame, heat loss and chamber pressure were explained.

From the viewpoint of various studies, for the measurement and calculation of the temperature near the side wall of the combustor and the heat transfer and heat flux from the gas to the wall, the correct experimental method is to use the thermocouple in the wall of the combustor, and then measure the temperature near the side wall of the combustor and the heat flux from the gas to the wall of the engine by measuring the temperature at different depths. The simulation method can be divided into components according to the different entrances, one defines several components of the gas, without considering combustion, which are mostly derived from the results of the CEA calculation, another uses the calculated physical parameters of the gas for the definition. The final component is the combustion, which is calculated by simplifying the main one-step or multi-step chemical reactions. Bartz's formula is widely used in theoretical calculation. This method is mainly used to calculate steady-state heat flux.

2. Experimental Test

The injector of this liquid rocket engine is a single-swirl kerosene injector with 12 oxygen direct current injectors around it. The ignition mode is spark plug ignition. According to the installation requirements of the heat flux meter, a square combustion chamber with thermocouples and heat flux meters along the engine axis was designed, as shown in Figure 1. The oxygen/kerosene supply system for this experiment was designed as shown in Figure 2. In the experiment, the hole plate is used to control the mass flow. In order to obtain the exact thermal conditions of the engine wall, two experiments were carried out in this study. The experimental conditions are shown in Table 1. After the installation of the experimental system, each side of the engine is shown in Figure 3.

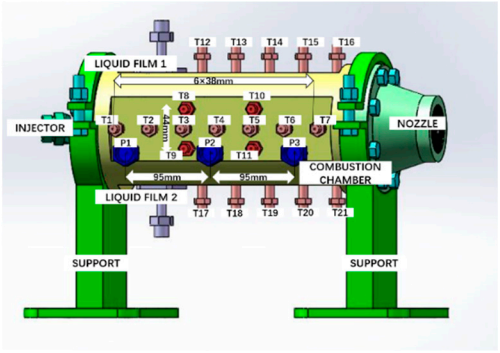

Figure 1. Experimental engine model.

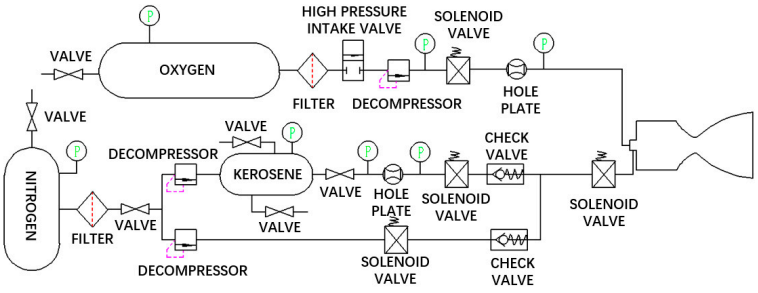

Figure 2. Experimental device system.

Table 1. Experimental conditions.

Parameters	Value
Pc/MPa	1.7
Mass flow/g/s	120
O/F	1
Throat diameter/mm	12
Carbon deposit	Case A: no; Case B: yes

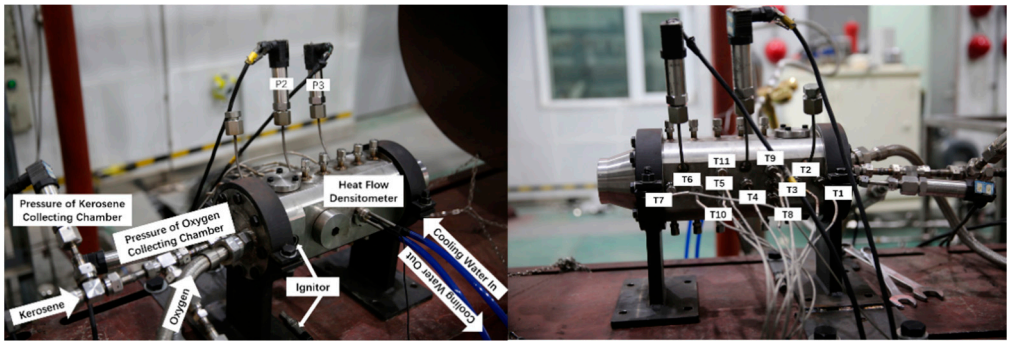

Figure 3. Experimental engine.

2.1. Axial Temperature Distribution

The pressure of the kerosene tank, oxygen collecting tank and kerosene collecting tank were monitored to determine whether the supply system has achieved the function of stabilizing the supply of fuel and oxygen.

Figure 4 shows that the pressure values remain constant in the normal working section of the combustion chamber, which indicates that the system works normally in the working stage of the engine. During this test, the chamber pressure value was 1.43 MPa, which was lower than the design value. This was mainly due to the large amount of carbon deposited in the combustion process. According to the ideal gas assumption, it was estimated that

84% of the combustion products in the combustion chamber were gas and 16% were carbon particles, meaning that the formation rate of the carbon deposit was 19.2 g/s. In addition, heat transfer will also cause combustion chamber pressure reduction in the actual process.

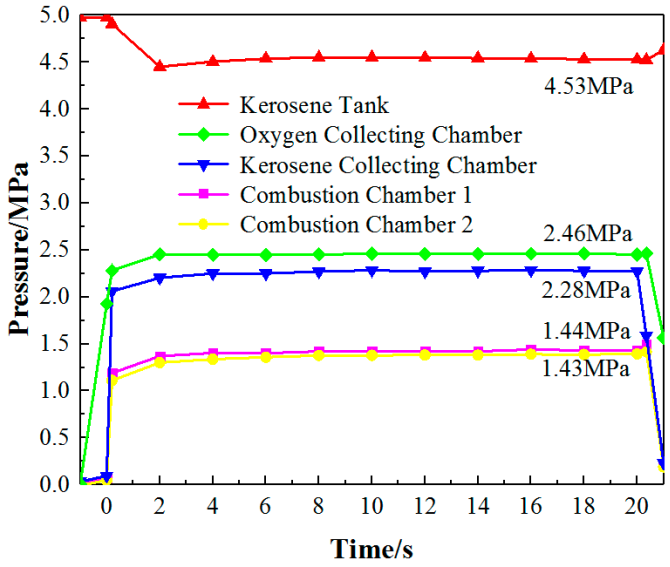

Figure 4. The main pressure monitoring points.

By monitoring the temperature distribution along the axis, the temperature distribution along the axis (as shown in Figure 5) and the temperature variation along the monitoring points with time (as shown in Figures 6 and 7) can be obtained when the heat transfer of the combustion chamber wall reaches a steady state. The distances between the monitoring points and the head are shown in Table 2.

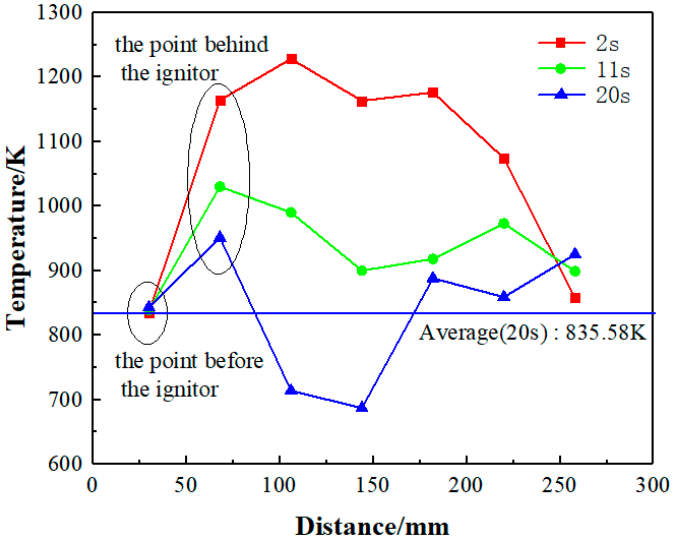

Figure 5. The temperature along the axial direction of gas side wall.

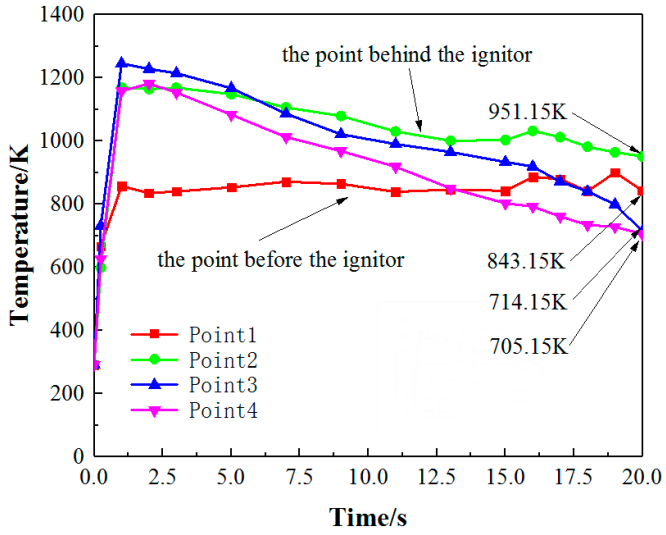

Figure 6. The temperature of the points 1–4.

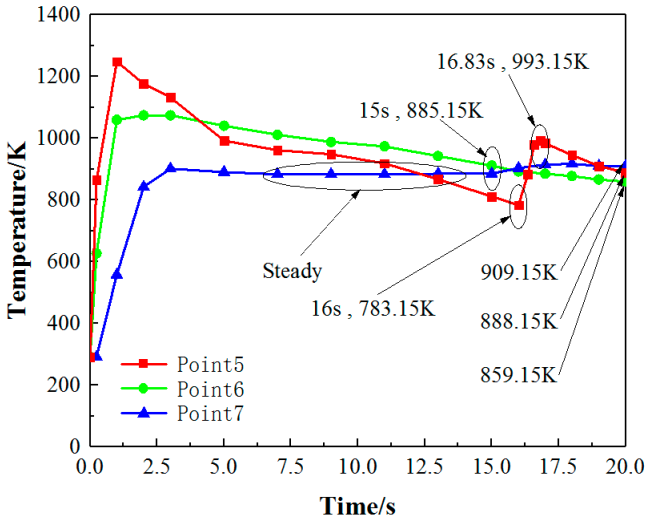

Figure 7. The temperature of the points 5–7.

Table 2. The distance of the monitoring points from the inlet.

The Number of the Point	The Distance from the Inlet/mm
1	30
2	68
3	106
4	144
5	182
6	220
7	258

It can be seen from Figure 5 that after 20 s of engine operation, the temperature measured at the monitoring point in front of the igniter is the closest to the average value, the temperature measured at the nearest monitoring point after the igniter is the highest, whereas the temperature at monitoring points 3 and 4 is the lowest. Then, at monitoring points 5 and 6 the temperature rises to the average temperature; at the monitoring point 7, the temperature rises slightly, which is mainly due to the fact that the temperature at monitoring point 7 increases slightly. Because there is no smooth square circle transformation

between the combustion chamber and the nozzle, a convex platform is formed here, which leads to the stagnation of flow to a certain extent and even the increase of static temperature.

The temperature values monitored are approximately the same at the time when the igniter has just finished its work. With time passing by, the temperature drops at monitoring points 2–6 to varying degrees, and in the first 11 s the temperature drops are roughly the same, which is mainly due to the gradual formation of the temperature boundary layer. After 11 s, the temperature of monitoring points 3 and 4 decreased more than the other points. There are two different reasons for this phenomenon. One is mainly due to the lack of combustion heat release in the region. The temperature of the bottom boundary layer was mainly developed from the upstream. During this period, the gas was continuously transferred to the wall, resulting in a lower temperature of the gas at the wall. After monitoring point 4, the combustion heat release process is again carried out, so the gas temperature at the wall rises after this point. The other reason is due to the high heat flux near monitoring points 3 and 4. According to the design of the oxygen direct injectors, the velocity of the oxygen near the injector is about 120 m/s, which can influence the heat transfer in the chamber greatly, especially the part near the injector. For this reason, the temperature of the main gas is the same but the heat transfer at points 3 and 4 is much higher than for points 5, 6 and 7. Which means the temperature difference is greater and the temperature of points 3 and 4 is lower.

It can be seen from Figures 6 and 7 that the monitoring points at different locations have different trends. The temperature of monitoring point 1 remains basically constant and fluctuates during the whole combustion chamber stage. Therefore, it can be analyzed that the flow and heat release are relatively stable. In addition, there is no initial peak and subsequent temperature drop in the whole process of the combustion chamber, which means the temperature at this point should be in the mixing atomization zone, where kerosene atomization, evaporation and thermal feedback from the back of the combustion chamber exist. There are initial peaks and subsequent temperature declines at monitoring points 2 to 6. This is mainly due to combustion at this stage. At the beginning of engine operation, high-temperature gas is produced by combustion, which moves to the periphery in the process of axial flow, so the temperature of the combustion chamber wall is higher at the initial stage. However, as time passes, the temperature boundary layer is gradually formed, so the temperature decreases gradually after 2 s. In Figure 6, the temperature fluctuation occurs at monitoring point 5 at 16 s, but the signal of the heat flux densitometer does not show this phenomenon (see Figure 8). Therefore, the reason for this phenomenon is that the carbon deposit is attached to the thermocouple head during the working process of the engine. At 16 s, the carbon layer falls off, resulting in local flow disturbance, and the temperature boundary layer is temporarily broken, and then quickly recovered.

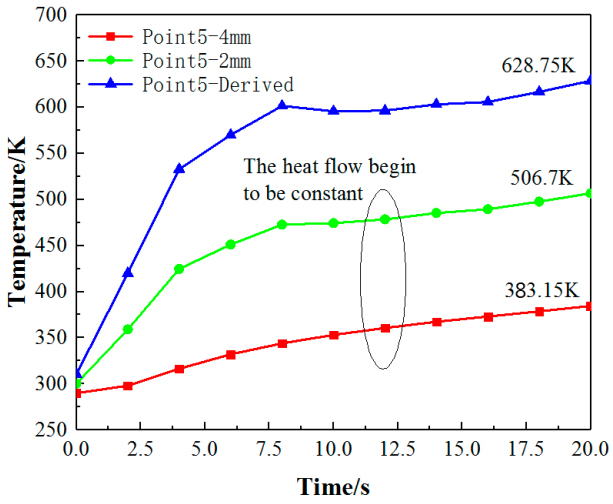

Figure 8. The temperature of the points in the wall.

2.2. Heat Flux Measurement

This experiment also monitored the temperature at 2 mm and 4 mm in the wall, as compared with monitoring point 5. As shown in Figure 8, the temperature increases gradually in the first 10 s, but the rising rate decreases gradually.

After 12 s, the rising rate of the two points is basically same, which means that the difference between them is constant while the heat flux in the combustion chamber wall remains constant. The variation of gas temperature at the wall temperature with time is calculated using the equation:

$$q = \frac{\lambda}{\delta}\Delta T \tag{1}$$

The results show that when the engine works for 20 s, the measured wall temperature of the gas reaches 628.75 K, which is lower than the gas temperature at the wall (885.15 K). The main reasons for this phenomenon are as follows.

(1) The temperature of the gas near the wall of the engine itself is slightly higher than the gas temperature at the wall.
(2) The heat flux obtained by using the temperature of 2 mm and 4 mm and Fourier's law is low, because the closer the distance between the monitoring points and the wall, the bigger the temperature gradient in the inner wall of the engine is.
(3) A carbon layer is attached to the thermocouple that monitors the gas temperature at the wall. On the one hand, the carbon layer separates the thermocouple from the gas side wall, making the temperature measured by the thermocouple lower than the gas temperature at the wall. On the other hand, the carbon layer increases the roughness of the thermocouple head and increases the heat transfer.

As shown in Figure 9, the heat flux at monitoring point 5 was measured directly by heat flux meter, and the influence of the carbon layer on the heat flux measurement was compared. The results show that the heat flux decreases at a constant rate between 6 s and 16 s. After 16 s, the heat flux tends to be constant. The measured heat flux is 0.937 MW/m^2 when there is no carbon deposit in the initial condition, and 1.001 MW/m^2 when there is carbon deposited in the initial condition, which is about 6.8% higher. The results show that the surface roughness of the heat flux meter increases with the existence of carbon deposit layer, which enhances the heat transfer of the gas to the heat flux meter.

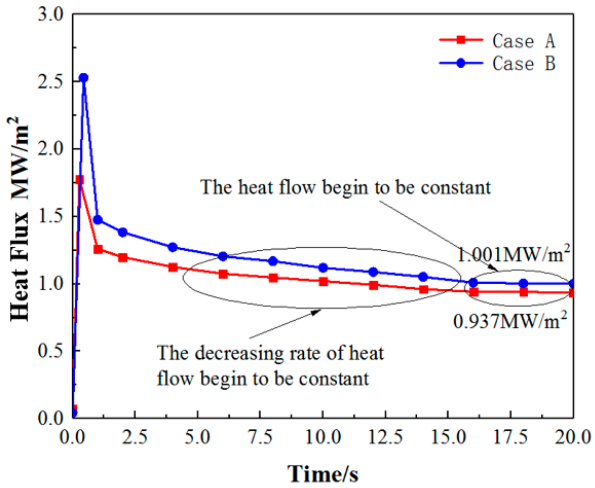

Figure 9. The heat flux of point 5.

3. Steady-State Calculation of Zero-Dimensional Wall Heat Flux

The combustion in the liquid rocket engine is complex and the physical and chemical properties of different regions are different. From the engine head to the nozzle, the combustion chamber can be divided into three zones: atomization zone, evaporation zone and mixing combustion zone. In order to simplify the theoretical calculation process, it is

necessary to simplify properly the combustion process of a rocket. Therefore, the following assumptions are adopted.

(1) Gas is evenly distributed along the circumference of the engine.
(2) Gas is in chemical equilibrium in the combustion chamber.
(3) The gas components distribute uniformly along the axial and radial directions, without considering the change of pressure with the axial position.

3.1. Thermodynamic Calculation

The chemical reactions of the gaseous oxygen/kerosene propellant combined engine are complex, and there are many kinds of gas components, up to dozens of kinds. In this paper, NASA CEA (chemical equilibrium with application) is used to calculate the main physical property parameters and components of gas. The experimental conditions (kerosene: JP10) were used to set up the calculation. The main parameters of the calculated gas are shown in Table 3 and the main components are shown in Table 4.

Table 3. Main physical property parameters of gas.

The Name of the Parameters	The Number of the Parameters
Temperature T_0/K	1764.65
Pressure p_c/Pa	1,700,000
Characteristic velocity C_{th}*/m/s	1471.19
Constant pressure specific heat ratio C_p/(kJ/(kg·K))	2.5637
Prandtl number	0.4824
Dynamic viscosity μ/(kg/(m·s))	5.75×10^{-5}
Specific heat ratio k	1.2878
Density ρ (kg/m^3)	1.776

Table 4. Main components of gas.

Components	Mole Fraction
H_2	0.48413
CO	0.44640
C(gr)	0.06390
CH_4	0.00376
H_2O	0.00134
CO_2	0.00034

3.2. Convection Heat Transfer

The convective heat transfer between the near wall gas and the engine wall is calculated using the basic Equation (2):

$$q_c = h_g\left(T_{aw} - T_{wg}\right) \tag{2}$$

The convection heat transfer coefficient is related to gas composition and physical and chemical properties. Different types of injectors will also lead to different combustion types in the combustion chamber, which will lead to a change in the convection heat transfer coefficient.

In simplified calculations, the influence of combustion details and other factors is neglected. The uniform gas assumption is adopted in the calculation model, and the convective heat transfer coefficient between near-wall gas and engine wall is calculated by using the modified formula (3), namely Bartz correlation [16]. The definition of T_0, p_c, C_p, μ, C^*_{th} is shown in Table 3.

$$h_g = \left[\frac{0.026}{d_t^{0.2}} \times \frac{\mu^{0.2} C_p}{Pr^{0.6}} \times \left(\frac{p_c}{C^*_{th}}\right)^{0.8}\right]\left(\frac{A_t}{A}\right)^{0.9}\delta \tag{3}$$

δ is a correction factor for introducing the effect of the change of the transverse flow property of the boundary layer on the heat transfer coefficient. Its calculation formula is as shown.

$$\delta = \left[\frac{T_{wg}}{2T_0}\left(1+\frac{k-1}{2}Ma^2\right)+\frac{1}{2}\right]^{-0.68}\left(1+\frac{k-1}{2}Ma^2\right)^{-0.12} \quad (4)$$

Because Bartz correlation is based on the empirical formula of turbulent boundary layers, the Reynolds number of combustion chamber flow should be calculated before use. The object of this study is a square combustor, so after it is equivalent to a cylindrical combustor, the calculation method of the Reynolds number of tube flow is used. The calculation formula is as shown.

$$Re = \frac{dV}{\nu} \quad (5)$$

The Reynolds number of the gas in the tube is 672,000. Therefore, the gas in the combustor is considered to be turbulent, meaning the convective heat transfer coefficient can be solved by Bartz correlation.

3.3. Radiation Heat Transfer

The formula for calculating radiant heat flux of uniform gas is still used (6):

$$q_r = \varepsilon_{w,ef}\sigma\left(\varepsilon_g T_0^4 - a_w T_{wg}^4\right) \quad (6)$$

The material used in this research is 1Cr18Ni9Ti, so the blackness of this material is 0.4 [17].

Simplified formula (7) is used to estimate the effective blackness of the wall.

$$\varepsilon_{w,ef} = \frac{1-\varepsilon_w}{2} \quad (7)$$

After substituting data, the value is 0.3. Considering the existence of a large amount of carbon black in the experimental process, the blackness of the gas is determined to be 1. Assuming that the gas side wall can be regarded as diffuse ash, that is, the absorption ratio and blackness are constant at a certain temperature, and the absorption ratio and blackness are consistent at the same temperature [18].

$$a_w = \varepsilon_w \quad (8)$$

3.4. Total Heat Flux Calculation and Correction

The total heat flux of the gas to the side wall of the engine, q, is the sum of convective heat flux and radiative heat flux.

$$q = q_c + q_r \quad (9)$$

As shown in Figure 7, the data measured at point 7 is relatively stable, so it is assumed that the temperature of the gas side wall is 885.15 K, the total heat flux of the gas to the wall is 0.57 MW/m^2 and the radiation heat flux accounts for 28.1% of the total heat flux (generally 15–20% [19]).

In the process of theoretical calculation, because the total temperature of gas used is calculated by CEA, it should be higher than the actual value, and the assumed velocity of gas in combustion chamber is Mach 0.3, which is also a high estimate. In the calculation of radiation heat flux, the assumed radiation rate of the gas is also a high estimate. However, the final calculation result is that the theoretical value is lower than the experimental result (0.937 MW/m^2).

The main reasons for this phenomenon are as follows.

(1) Theoretical calculation does not take into account the increase in the roughness of combustion chamber wall caused by carbon deposition.

(2) The momentum diffusion ability of gas is reduced and the heat diffusion ability improved due to the absence of a large number of carbon particles with high thermal conductivity in the gas, that is, a high Pr number is brought in, which leads to the low calculated convective heat-transfer system.

In order to consider the influence of the high thermal conductivity of the carbon particles, we need to correct the Pr number by volume fraction of carbon deposition. According to the quality of the carbon deposition estimated by the last part, it is easy to get the volume fraction of carbon deposition, which is 0.01732%. Choosing the thermal conductivity of sedimentary graphite (539 W/(m·K)) to represent the value of the carbon particles, the new thermal conductivity of the whole gas is 0.124 W/(m·K) and the Pr number is changed to 0.1206. At this time, the total heat flux of the gas to the wall is 1.11 MW/m^2, and the radiation heat flux accounts for 14.5% of the total heat flux. This theoretical value is more similar to the experimental result.

4. Numerical Simulation of the Fluid Part

4.1. Model Simplification and Numerical Simulation

According to the experimental result, the gas temperature at the wall begins to be constant with time passing by. Therefore, the constant temperature boundary can be used in the numerical simulation of the fluid to study the heat flux of the combustion chamber.

The numerical simulation in this paper is mainly carried out on the ANSYS fluent. The governing equations are discretized and solved by the finite volume method. The coupled algorithm is used to deal with the coupling problem of velocity and pressure. The convection term is discretized by the second-order upwind discretization method, and the viscous term is discretized by the central difference scheme.

Because of the axisymmetric configuration of the thrust chamber, the simulation was carried out only for 90° in the circumferential direction assuming the symmetry condition at the circumferential boundaries. Figure 10 shows the grid scheme of the numerical methodology, hexahedral mesh was used as grid topology in the hot-gas region. For a good resolution of the boundary layer that develops along the coupling interface, the grids were clustered in the vicinity of coupling interface with wall y+ between 30 and 300. Grid independence had been verified by comparing the calculated results of pressure, as shown in Figure 11, and the final number of grids is about 550,000. These computational grids were generated using the software ICEM.

Fixed total conditions were used at the inlet of the thrust chamber, the total pressure was 1.7 MPa, total temperature was 1819.24 K and total mass flow rate was 0.03 kg/s. The mass fractions of each chemical species at thruster were calculated by the calculation program CEA and shown in Table 4. The chamber wall was treated as a non-slip, adiabatic boundary with 885.15 K and the outlet boundary was set as 0.1 MPa.

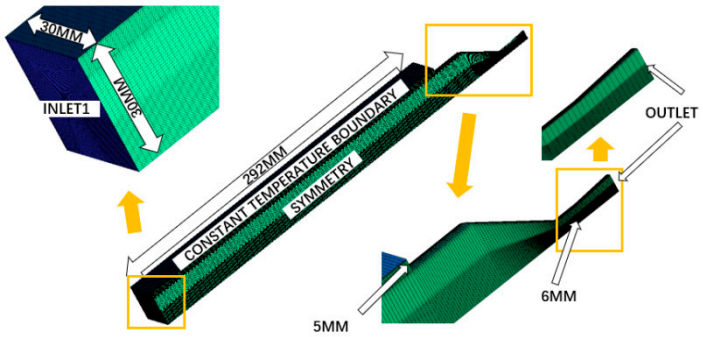

Figure 10. The mesh of the fluid part (without considering injectors).

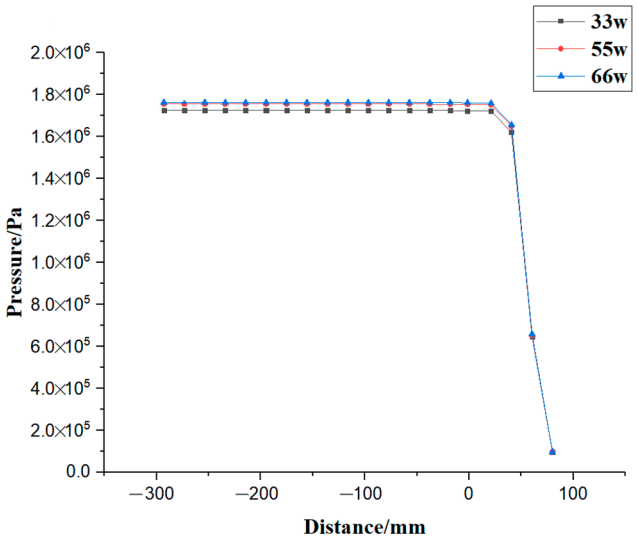

Figure 11. The mesh independence verification results.

In addition, there are two reasons which could cause the phenomenon of the temperature along the axial direction of gas side wall. To analyze which one is the correct we simulate the fluid part with the structure of the injector. If the simulation result is similar to the result of the experiment, it means that the initial kinetic energy caused the phenomenon of the temperature along the axial direction of the gas side wall. Otherwise, the different regions of combustion heat release are the main reason. The mesh of the fluid part (considering injectors) is shown in Figure 12. After adding the injector structure, the number of grids is about 58 w, and the boundary conditions are the same as those without the injector.

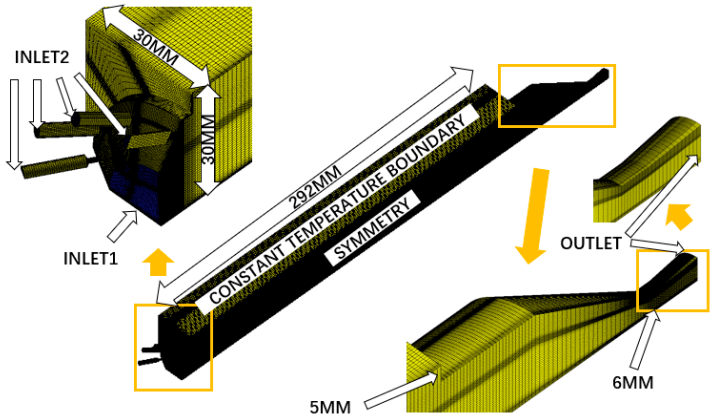

Figure 12. The mesh of the fluid part (considering injectors).

These simulations only use the gas heat property parameters from the CEA (the thermal conductivity is 0.124 W/(m·K), which is corrected by considering the carbon deposit).

4.2. Numerical Simulation Result

The cloud pictures of the simulation without considering injectors are shown in Figure 13. The temperature cloud picture show that the temperature boundary layer of gas does not form at the entrance and then turns to be thickened. Because of a convex platform near the nozzle, the temperature boundary layer becomes thickest. This convex platform is used to simplify the model and let it easily mesh. This result shows that the convex platform will not influence the phenomenon at monitoring point 5, and therefore it can be used.

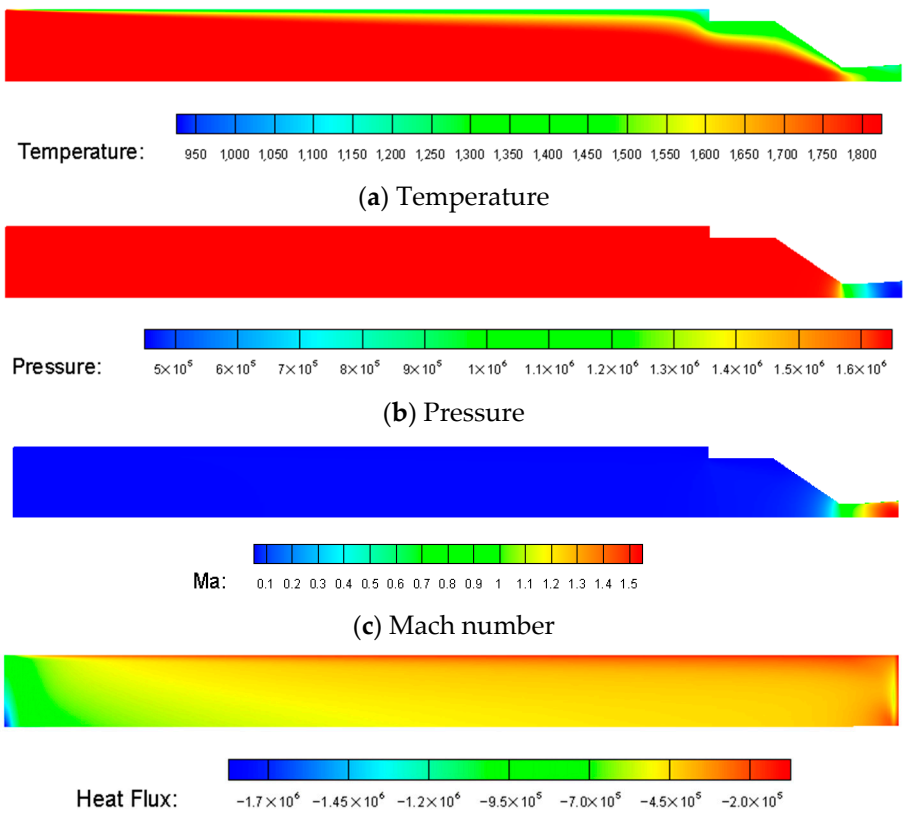

(**a**) Temperature

(**b**) Pressure

(**c**) Mach number

(**d**) Heat flux of the gas side wall

Figure 13. The cloud pictures of the simulation (without considering injectors).

From the pressure cloud picture, the pressure in the chamber is about 1.7 MPa, which is the same as the theoretical design parameter but is higher than the experimental result (1.44 MPa). That is the result without considering the carbon particles in the chamber. Additionally, the pressure and Mach number cloud pictures can prove that the engine works well.

The heat flux cloud picture of the gas side wall is shown in Figure 13d, and the heat flux along the axial direction of gas side wall is in Figure 13. From these two pictures, the heat flux turns to be high at the entrance, this is caused by the unformed temperature boundary layer. But at point 5 (182 mm), the heat flux turns to be constant, as shown in Figure 14. Defining the heat flux there is the convection heat flux, and then, plus the theoretical radiation heat flux, the total heat flux is 0.63 MW/m^2, which is lower than the experimental result.

The cloud pictures of the simulation considering injectors are shown in Figure 15. The temperature cloud picture does not show the same temperature boundary layer as the simulation result (without considering injectors), in fact, the temperature boundary layer is much thinner and the static temperature of the main flow is not constant until the point (249 m). From the pressure cloud picture, the pressure in the chamber is about 1.7 MPa which is the same as the simulation result (without considering injectors), but the Mach number cloud picture shows differences. Because of considering the injectors, the *Ma* at the entrance is inhomogeneous, and in the middle the *Ma* (0.05) is higher than the last one (0.019), which leads to the high heat flux.

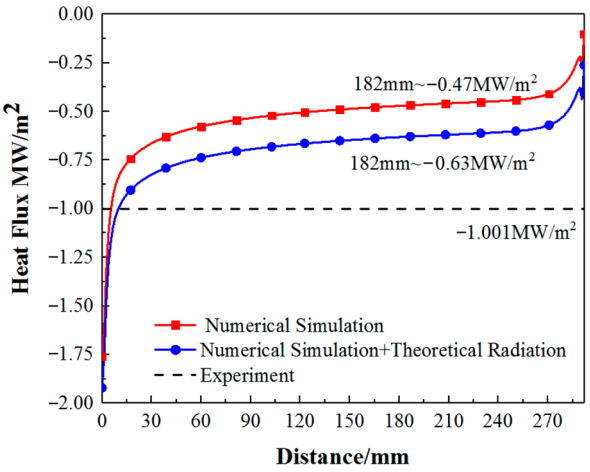

Figure 14. The heat flux along the axial direction of gas side wall (without considering injectors).

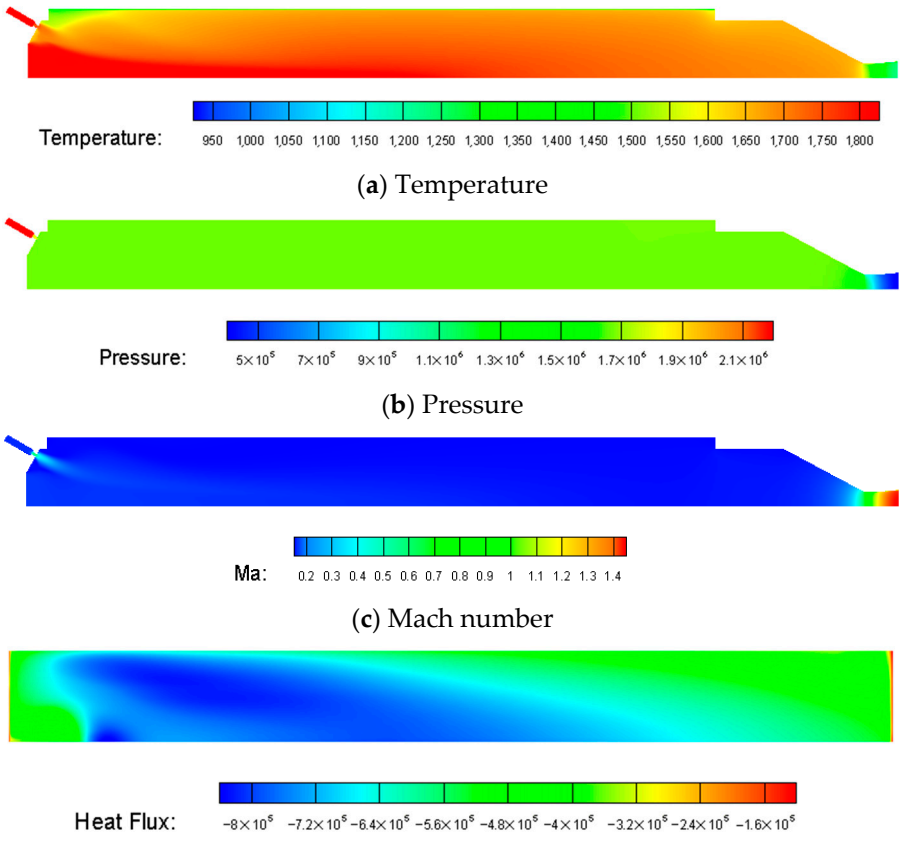

Figure 15. The cloud pictures of the simulation (considering injectors).

The heat flux cloud picture of the gas side wall is shown in Figure 15d, and the heat flux along the axial direction of gas side wall is in Figure 15. From these two pictures, the heat flux is lowest at the entrance, and then improves rapidly. This is because there is a low speed and low static temperature zone near the entrance. Additionally, the static temperature of the flow from inlet2 is lower than the flow from inlet1. When they feed into the chamber, the static temperature of the flow from inlet2 turns to be higher by mixing, which leads to the slow improvement from 51.4 mm to 130 mm. Then, the heat flux decreases slowly because the *Ma* number from 130 mm to the convex platform is not as high as at the entrance and the static temperature turns to be lower. Adding the theoretical

radiation heat flux, the total heat flux of point 5 (182 mm) is 0.89 MW/m^2, which is similar to the experimental result. This means that using the corrected thermal conductivity and the model considering the injector, the result can be in good agreement with the experiment.

As for the two explanations for the phenomenon of the temperature along the axial direction of gas side wall, it can be confirmed by comparing the result using Bartz's formula and the result of the simulation, shown in Figure 16. The curve shows different temperature distributions, therefore, the initial kinetic energy of the gas from the oxygen direct injectors is not the main reason for the phenomenon; therefore, the explanation that there are three combustion and heat release zones is correct.

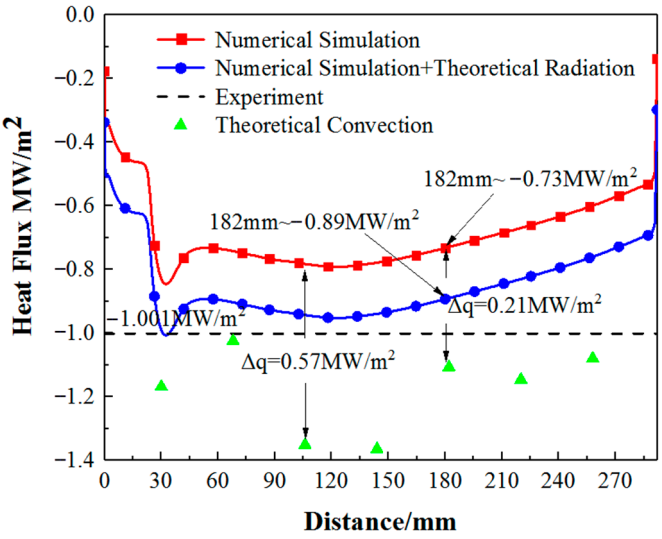

Figure 16. The heat flux along the axial direction of gas side wall (considering injectors).

5. Conclusions

In this paper, a liquid rocket engine is taken as the research object. The temperature distribution along the axis of the engine is measured by thermocouples. The heat flux at monitoring point 5 is measured using a heat flux meter. In this paper the effect of carbon deposition on heat transfer is analyzed. This paper also compares and analyses the accuracy of the results obtained by theoretical calculation and numerical simulation results. The main conclusions are as follows:

(1) Under these conditions, there are three areas in the combustion chamber, namely, the mixing atomization zone, the first combustion heat release zone and the second combustion heat release zone.

(2) The existence of a carbon deposit layer leads to an increase in the surface roughness of testing equipment under these conditions, making the measured value of the testing equipment 1.001 MW/m^2, which is about 6.8% higher than the measured value of 0.937 MW/m^2 without carbon deposition layer.

(3) After the thermal conductivity is corrected by estimating the volume fraction of carbon deposition, the calculated result rises to 1.11 MW/m^2, which has an error of 10.1% with the experimental measured value with carbon deposition. After considering the influence of injectors, the result of numerical calculation is 0.89 MW/m^2, which has an error of 5% with the experimental value without carbon deposition. The above results show that the calculation error with or without carbon deposition can be reduced by correcting the thermal conductivity and considering the injectors.

Author Contributions: Conceptualization, X.W. and Z.Z.; methodology, Z.Z.; validation, X.W., Z.Y. and J.Y.; writing—original draft preparation, X.W. and S.Z.; writing—review and editing, O.J.H.; funding acquisition, X.W. and S.Z. All authors have read and agreed to the published version of the manuscript.

Funding: This work was supported by the National Natural Science Foundation of China (Program No. 52006181), Natural Science Basic Research Program of Shaanxi (Program No. 2021JC-14) and Key Research and Development Program of Shaanxi (Program No. 2019ZDLGY19-09).

Institutional Review Board Statement: Not applicable.

Informed Consent Statement: Not applicable.

Data Availability Statement: Not applicable.

Acknowledgments: The first author is sponsored by China Scholarship Council and Top International University Visiting Program for Outstanding Young Scholars of Northwestern Polytechnical University.

Conflicts of Interest: The authors declare no conflict of interest.

Nomenclature

q_c	heat flux, W/m^2
h_g	convective heat transfer coefficient, W/(m^2·K)
T_{aw}	adiabatic wall temperature, K
T_{wg}	wall temperature near gas, K
d_t	diameter of the throat, m
A_t	area of the throat, m^2
A	area of the combustor, m^2
δ	correction factor
k	specific heat ratio of gas
Ma	Mach number in combustion chamber
d	equivalent diameter of combustion chamber, m
V	gas axial velocity, m/s
ν	kinematic viscosity of gas, m^2/s
q_r	radiant heat flux, W/m^2
$\varepsilon_{w,ef}$	effective blackness of the wall
σ	Stephen–Boltzmann constant, 5.67×10^{-8} W/(m^2·K^4)
ε_g	blackness of gas
ε_w	blackness of wall
a_w	wall absorptivity

References

1. Song, J.; Sun, B. Thermal-structural analysis of regeneratively-cooled thrust chamber wall in reusable LOX/Methane rocket engines. *Chin. J. Aeronaut.* **2017**, *30*, 1043–1053. [CrossRef]
2. Höglauer, C.; Kniesner, B.; Knab, O.; Schlieben, G.; Kirchberger, C.; Silvestri, S.; Haidn, O.J. Modeling and simulation of a GOX/kerosene subscale rocket combustion chamber with film cooling. *CEAS Space J.* **2015**, *7*, 419–432. [CrossRef]
3. Suslov, D.; Arnold, R.; Haidn, O. Investigation of Two Dimensional Thermal Loads in the Region Near the Injector Head of a High Pressure Subscale Combustion Chamber. In Proceedings of the 47th AIAA Aerospace Sciences Meeting including The New Horizons Forum and Aerospace Exposition, Orlando, FL, USA, 5–8 January 2009.
4. Arnold, R.; Suslov, D.; Haidn, O. Circumferential film cooling effectiveness in a LOX/H2 subscale combustion chamber. *J. Propul. Power* **2009**, *25*, 760–770. [CrossRef]
5. Wang, T.; Sun, B.; Liu, D.; Xiang, J. Experimental investigation of two-dimensional wall thermal loads in the near-injector region of a film-cooled combustion chamber. *Appl. Therm. Eng.* **2018**, *138*, 913–923. [CrossRef]
6. Pizzarelli, M.; Betti, B.; Nasuti, F. Coupled analysis of hot-gas and coolant flows in LOX/methane thrust chambers. In Proceedings of the 4th European Conference for Aerospace Sciences, Saint Petersburg, Russia, 4–8 July 2011.
7. Lai, Y.G.; Przekwas, A.J.; Nguyen, N. *A Concurrent MuIti-Dsicipiinary Approach for the Analysis of Liguid Rocket Engine Combustors*; AIAA: Reston, VA, USA, 1994.
8. Negishi, H.; Kumakawa, A.; Yamanishi, N.; Kurosu, A. Heat transfer simulations in liquid rocket engine subscale thrust chambers. In Proceedings of the 44th AIAA/ASME/SAE/ASEE Joint Propulsion Conference & Exhibit, Hartford, CT, USA, 21–23 July 2008.
9. Song, J.; Sun, B. Coupled numerical simulation of combustion and regenerative cooling in LOX/Methane rocket engines. *Appl. Therm. Eng.* **2016**, *106*, 762–773. [CrossRef]
10. Betti, B.; Pizzarelli, M.; Nasuti, F. Coupled Heat Transfer Analysis in Regeneratively Cooled Thrust Chambers. *J. Propuls. Power* **2014**, *30*, 360–367. [CrossRef]

11. Celano, M.P.; Slivestri, S.; Pauw, J.; Perakis, N.; Schily, F.; Suslov, D.; Haidn, O.J. Heat Flux Evaluation Methods for a Single Element Heat-Sink Chamber. In Proceedings of the 6th European Conference for Aeronautics and Space Sciences (EUCASS), Krakov, Poland, 29 June–3 July 2015.
12. Suslov, D.; Betti, B.; Aichner, T.; Soller, S.; Nasuti, F.; Haidn, O. Experimental Investigation and CFD-Simulation of the Film Cooling in an O2/CH4 subscale Combustion Chamber. In Proceedings of the Space Propulsion 2012, Bordeaux, France, 7–10 May 2012.
13. Ma, P.C.; Wu, H.; Ihme, M.; Hickey, J.-P. A flamelet model with heat-loss effects for predicting wall-heat transfer in rocket engines. In Proceedings of the 53rd AIAA/ASME/SAE/ASEE Joint Propulsion Conference, Atlanta, GA, USA, 10–12 July 2017.
14. Maestro, D.; Cuenot, B.; Selle, L. Large Eddy Simulation of flow and combustion in a single-element GCH4/GOX rocket combustor. In Proceedings of the 7th European Conference for Aeronautics and Space Sciences (EUCASS), Milan, Italy, 3–7 July 2017.
15. Maestro, D.; Cuenot, B.; Selle, L. Large Eddy Simulation of Combustion and Heat Transfer in a Single Element GCH4/GOx Rocket Combustor. *Flow Turbul. Combust.* **2019**, *103*, 699–730. [CrossRef]
16. John, J.E.; Ronald, F.Z. *Thrust Chamber Life Prediction. Volume 1: Mechanical and Physical Properties of High Performance Rocket Nozzle Materials*; NASACR: Daytona Beach, FL, USA, 1975.
17. Zhang, Z.; Zhang, M.; Zhou, L. *Thermal Protection of Liquid Rocket Engines*; National Defense Industry Press: Beijing, China, 2016.
18. Yang, S.; Tao, W. *Heat Transfer*; Higher education press: Beijing, China, 2006.
19. Yang, L.; Fu, Q. *Design of Thrust Chamber for Liquid Rocket Engine*; Beijing University of Aeronautics and Astronautics Press: Beijing, China, 2013.